Nonlinear Responses of Vegetation Phenology to Climate Change and Urbanization: A Case Study in Beijing, China

Jiahui Yao and Haiyong Ding

***Abstract*—Vegetation serves as an indicator of ecological change, and phenology is an important indicator for evaluating vegetation growth and development. Analyzing the spatiotemporal characteristics of vegetation phenology and its driving factors is of great significance for analyzing the carbon, water, and energy balance of terrestrial ecosystems. To better assess the impact of external environmental changes on vegetation phenology and comprehend the changing trends of phenology, this study employed phenological parameters as response variables and incorporated meteorological and urbanization factors as explanatory variables. A generalized additive model (GAM) was constructed meticulously to investigate how vegetation phenology responds to climate change and urbanization in Beijing, as well as to predict vegetation phenology. The results showed that there were nonlinear relationships between the vegetation phenological parameters, i.e., start of season (SOS) and end of season (EOS), and external environmental changes. R^2 of the GAM predicted SOS and EOS with respect to the observed data increased to 0.622 and 0.756, respectively. The prediction effects in each region of the urban–rural gradient zone were better with the root-mean-square error of approximately 4–7 days. This study demonstrates that the GAM considers the nonlinear relationships between vegetation phenology and external environmental factors. The validation results based on the observed data show that the models are reliable, and the findings can provide theoretical references for urban development planning and ecological environmental protection in Beijing.**

***Index Terms*—Climate change, generalized additive model (GAM), urbanization, vegetation phenology.**

I. Introduction

VEGETATION is the most important component of terrestrial ecosystems [1]. It plays an important role in the global carbon cycle and energy conversion [2] and is a sensitive indicator for monitoring global environmental changes at different temporal and spatial scales. Vegetation phenology describes the cyclical natural change process, including budding, flowering, maturity, defoliation, and dormancy, throughout the year [3]. Changes in vegetation phenology are an important response of ecosystem dynamics to climate and environmental changes [4]. The driving factors of phenological changes mainly include the environmental (climate, soil, and biology) and management measures [5], among which climate change is one of the most important factors affecting vegetation growth and development and is the basis for plant morphological construction and physiological and biochemical changes [6]. At the same time, urbanization is developing rapidly, which has become one of the biggest challenges of this century [7]. Urbanization has had a certain impact on vegetation growth and development, which can affect vegetation phenology by changing environmental factors in urban areas, including hydrology, light, air pollutants, and urban heat islands [8]. While changing the original land cover and land use status, urban areas also affect the climate conditions and ecological elements of local areas. The observed rising of temperature in urban areas exceeds the projected global temperature rise in the coming decades [8]. Differences in land surface temperature in urban and rural areas are also one of the main factors affecting phenological changes [9], and changes in start of season (SOS) and end of season (EOS) are deeply affected by urban heat island intensity [10]. Different from the natural environment, the urban ecological environment is affected by both climate change and urbanization, so studying the changing patterns of urban vegetation phenology can provide insights into the possible impact of future climate change and urban ecological adaptation.

In recent years, the spatiotemporal characteristics of vegetation phenology and its responses to external environmental changes have attracted the attention of scholars. Most of the current studies have analyzed the impact of external environmental changes on vegetation phenology, assuming that there is a significant linear relationship between phenology and external environmental changes. Commonly analytical methods are mainly correlation analysis and linear regression analysis of statistical methods. However, in fact, the response of vegetation growth and development to the environment is a highly complex process, and simple linear relationships cannot explain the impact of external environment changes on vegetation growth and development [11]. Therefore, research on the analysis of the nonlinear relationships between vegetation phenology and external environmental changes is gradually increasing [12], [13], [14]. Meanwhile, nonlinear models have been used for vegetation phenology prediction, which are suitable for exploring the nonlinear impact of large-scale climate change on phenology [15], and the

Manuscript received 6 November 2023; revised 27 December 2023 and 8 January 2024; accepted 9 February 2024. Date of publication 20 February 2024; date of current version 1 March 2024. This work was supported by the Major Project of High Resolution Earth Observation System under Grant 30-Y60B01-9003-22/23. This work was developed by the IEEE Publication Technology Department. *(Corresponding author: Haiyong Ding.)*

The authors are with the School of Remote Sensing and Geomatics Engineering, Nanjing University of Information Science and Technology, Nanjing 210044, China (e-mail: 20211248053@nuist.edu.cn; hyongd@163.com).

Digital Object Identifier 10.1109/JSTARS.2024.3367734

prediction accuracy using nonlinear models is higher [16], [17]. Motivated by these studies of using nonlinear models to predict phenology, this study proposes the application of the generalized additive model (GAM) to analyze the nonlinear relationships between vegetation phenology, climate change, and urbanization and evaluate the feasibility of vegetation phenology prediction. The GAM is data driven rather than model driven, does not need to assume the distribution of the data, and is highly useful in cases of multiple nonparametric responses. The GAM is capable of analyzing complex nonlinear relationships between dependent and multiple independent variables [18] and can also explain long-term trends in data [19], [20]. Therefore, it is well suited for the analysis of ecological data and widely used in ecology [21], pollution [22], [23], medicine [24], [25], and so on. In terms of phenology research, many researchers have used the GAM to analyze vegetation growth and development. White et al. [26] found that the accuracy of predicting the difference of SOS among different latitude zones by the GAM was about 2.4 days by using annual average temperature, urban vegetation coverage, and the difference of normalized difference vegetation index (NDVI) amplitude between urban and forest areas. Song and Cao [27] employed the GAM to analyze the relationships between topographic factors and vegetation richness in the central subtropical region of China, and they found that there was a significant correlation between the vegetation richness fitted by the GAM and the observed value. Younes et al. [28] used the GAM to create models for six different mangroves in Australia and analyze their responses to environmental variables and predicted phenological changes.

As far as we know, most of the current studies primarily focus on analyzing the response and feedback of vegetation phenology to external environmental changes, without achieving the objective of predicting phenology through a quantitative analysis of the relationship between phenology and external environmental variables. There was no such research on the prediction of vegetation phenology in Beijing under the background of climate change and rapid urbanization. Beijing is one of the fastest-growing and most densely populated cities in China, and it was found that the significant urban sprawl has had a considerable impact on the thermal environment, resulting in significantly higher temperature in the central urban areas than in surrounding rural areas [29]. Therefore, it is an ideal choice to explore the response of vegetation phenology to climate change and urbanization in Beijing. On this basis, this study extracted vegetation phenological parameters from the moderate resolution imaging spectroradiometer (MODIS) enhanced vegetation index (EVI) time-series products in Beijing from 2001 to 2020 and analyzed the spatial differences and interannual variations and trends of phenology in urban, suburban, and rural areas. Then, the nonlinear relationships between vegetation phenology and its driving factors were investigated, and the start and end times of vegetation phenology on the urban–rural gradient were predicted by the GAM. This study further evaluated the ability of the GAM to predict vegetation phenology and provided a theoretical basis for subsequent urban ecological sustainable development planning.

II. Study Area

Beijing is located at 115.7°–117.4°E, 39.4°–41.6°N, situated in the northern part of the North China Plain, adjacent to the Bohai Sea [see Fig. 1(a)]. It shares borders with Hebei Province, except for its eastern connection with Tianjin. Beijing has a higher elevation in the northwest and a lower elevation in the southeast [see Fig. 1(b)], surrounded by mountains on three sides. The climate is characterized as a warm temperate continental monsoon climate with distinct seasonal variations and rich vegetation cover [see Fig. 1(c)]. As the political, economic, and cultural center of China, Beijing is the core city of the Beijing–Tianjin–Hebei urban agglomeration. The city has experienced rapid economic development, and its urbanization level far exceeds that of other cities. The urban heat island effect resulting from urbanization is the main cause of local warming and has a certain impact on the vegetation phenology in the city. Therefore, it is of great significance to study the vegetation phenology in Beijing.

III. Materials and Methods

A. Data

The Terra Moderate Resolution Imaging Spectroradiometer Vegetation Indices (MOD13Q1) Version 6 product, with a spatial resolution of 250 m and a temporal resolution of 16 days, was used to detect vegetation phenology for the 2001–2020 period. The MOD13Q1 product contains two datasets: NDVI and EVI. The EVI dataset eliminates the influence of clouds and aerosols to a certain extent, which is more appropriate for monitoring vegetation dynamics in urban areas [9]. The fitted EVI curves were used to extract vegetation phenological parameters, which were widely used in monitoring and researching the dynamics of vegetation at different scales. The MCD12Q2 dataset[2] was employed to validate the extracted phenological parameters across the study area from 2001 to 2019. The dataset offered a spatial resolution of 500 m and a temporal resolution of one year.

The urban buffer zone boundaries were derived from the Chinese urban built-up area dataset published by He et al. [30]. This dataset extracted the built-up area of Chinese cities from 1992 to 2020, which can be used to assess the impact of urban expansion process on the natural environment and provide data support for understanding the process of urban expansion and its impact in China. The built-up area of each year was the urban area, and buffer zones of 0–5 km, 5–10 km, 10–15 km, 15–20 km, and 20–25 km were established outside the urban areas [31], of which 0–20 km were the suburban areas of the urban–rural gradient zone, and 20–25 km were the rural areas [9] (see Fig. 2).

The meteorological data were obtained from the China Climate Dataset V3.0 of the China Meteorological Science Data Sharing Service.[3] The dataset included temperature, sunshine hours, humidity, wind speed, precipitation, etc. The kriging interpolation method was used to interpolate the meteorological

[1] [Online]. Available: http://www.ncdc.ac.cn
[2] [Online]. Available: https://lpdaac.usgs.gov/
[3] [Online]. Available: http://data.cma.cn/

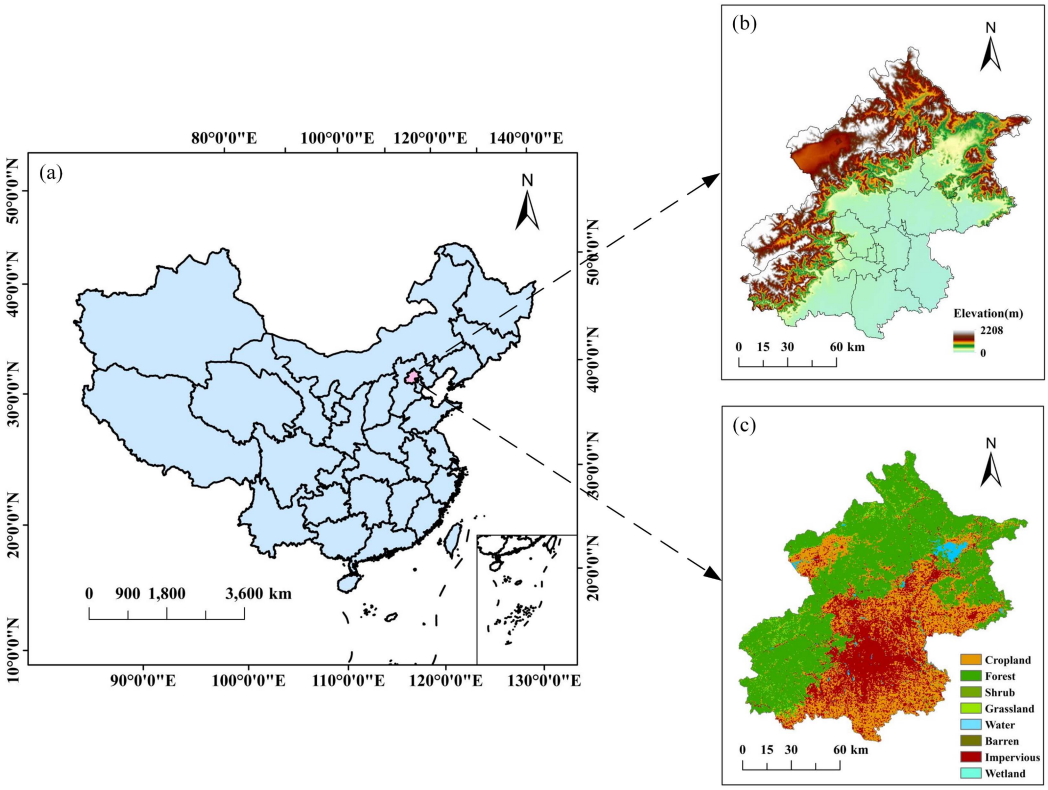

Fig. 1. (a) Location, (b) elevation, and (c) land cover classification of the study area. The land cover dataset is provided by the National Cryosphere Desert Data Center.[1]

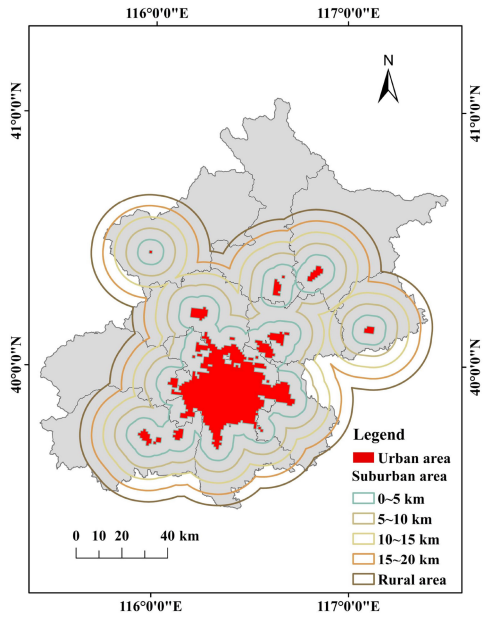

Fig. 2. Spatial distribution of urban areas and buffer zones in Beijing in 2001.

station data to form a raster dataset with a spatial resolution of 250 m consistent with the phenological data. In this study, the meteorological data from January to April and July to October of 2001–2020 were analyzed, and the data were removed when there were missing or abnormal values.

WorldPop[4] population density data provide gridded population data from 2000 to 2020 at a global resolution of 100 m and 1 km, and we used gridded population density data for Beijing from 2001 to 2020 at a spatial resolution of 100 m as a representation of urbanization. The new nighttime light dataset with a higher spatial resolution of 500 m has a similar quality to the national polar-orbiting partnership visible infrared imaging radiometer suite (NPP-VIIRS) nighttime light data and clearly reflects the detailed information of the inner city and its temporal variations [32]. The digital number (DN) value directly reflected the distribution, intensity, and temporal changes of light sources, providing reliable support for evaluating the intensity of human activities and urbanization. The urban heat island intensity data were obtained from MOD11A2,[5] which recorded the average surface temperature during eight days of clear weather with a 1000-m spatial resolution and was suitable for urban heat island intensity analysis.

To be consistent with the phenology data, all data projections were converted to WGS84 UTM Zone 50N and resampled to 250-m spatial resolution.

B. Methods

1) Extraction of Vegetation Phenological Parameters: Due to the influence of sensor characteristics and other external

[4][Online]. Available: https://worldpop.org/
[5][Online]. Available: https://lpdaac.usgs.gov/

factors such as cloud cover and atmospheric aerosols, there can be deviations between vegetation index data and the actual phenological growth patterns of vegetation seasons [33]. Therefore, it is necessary to reconstruct the original EVI data in a time series. In this study, the double logistic (D-L) function method was chosen to fit the EVI time-series data

$$f(t) = m_1 + m_2 \left(\frac{1}{e^{m_3 - m_4 t}} - \frac{1}{e^{m_5 - m_6 t}} \right) \tag{1}$$

where $f(t)$ is the fitted EVI value at day t, and $m_i (i = 1, \ldots, 6)$ are the fitted parameters.

The D-L function method does not require the determination of a threshold, and its local fitting is based on the variation characteristics of the EVI curve, and the fitted peak closely approximates the peak of the original EVI curve. This method is suitable for monitoring phenology at different vegetation-covered regions, and even at a global scale.

The threshold method determines vegetation phenological parameters by setting threshold conditions for the vegetation indices. It identifies the points on the vegetation index curve, where the amplitude reaches a certain proportion during the rising and falling phases as the start and end of the vegetation growing season [34]. In this study, we combined previous studies with practical considerations and set the threshold for extracting SOS as 0.2 and the threshold for extracting EOS as 0.4.

2) Generalized Additive Model: The GAM is a nonparametric extension of the generalized linear model, which is commonly used to explore nonlinear relationships between dependent and independent variables [18]. The GAM is a nonparametric regression model that utilizes additive functions, permitting both the linear and smooth functions fit for explanatory variables. It can automatically select appropriate degrees of freedom [35]. The mathematical expression of the GAM is

$$g(E(Y)) = \alpha + s_1(X_1) + s_2(X_2) + \cdots + s_p(X_p) \tag{2}$$

where g is a link function, $E(Y)$ denotes the mathematical expectation of the response variable, α is the constant intercept term, s_p is the nonparametric function explaining the relationship of the variables, and X_p is the predictor variable.

If all the variables are introduced into the prediction model, the model often gets disturbed by nonessential factors, resulting in an unreasonable significance of the parameter estimation or the loss of significance tests for some explanatory variables. Therefore, it is necessary to screen the variables and determine the input variables for the model. In this study, the GAM was employed for variable selection, and the Akaike information criterion (AIC) was used to assess the model fit [36]. The estimated degree of freedom can be interpreted as the smoothness of the predictor variable. When the estimated degree of freedom equals 1, there is a linear relationship between the explanatory and response variables. When the estimated degree of freedom is greater than 1, there is a nonlinear relationship between the explanatory and response variables. Larger values of degrees of freedom indicate stronger nonlinear relationships.

3) Explanatory Variable Preprocessing for the GAM: The univariate GAM was constructed first. A separate GAM was built to fit each physical response variable (SOS and EOS) with each explanatory variable (meteorological and urbanization variables). The model fitting was performed using the package mgcv in R [37]. Thin plate regression splines (the default in mgcv) were used as the smoothing function [38]. In the second step, explanatory variable selection was conducted. For each phenological response variable, a forward stepwise regression was performed by refitting the GAM with the explanatory variables selected in the first step. Each explanatory variable was gradually added to the model, and the overall deviance explained and AIC were recalculated. If the AIC decreased without a corresponding decrease in deviance explained, the explanatory variable was retained

$$\text{AIC} = n \cdot \ln \left(\frac{\sum_{i=1}^{n} (y_i - \hat{y}_i)^2}{n} \right) + 2q. \tag{3}$$

The GAM was constructed with SOS and EOS as response variables and with meteorological and urbanization factors as explanatory variables. Among the meteorological factors, precipitation, maximum temperature, minimum temperature, sunshine hours, wind speed, and humidity were selected to represent climate change. For urbanization factors, population density, nighttime light intensity, and urban heat island intensity were selected to represent urbanization. Most previous studies have primarily focused on climate change at annual or seasonal scales, overlooking the fact that phenological events are cumulative processes, and the dynamic changes in preseason meteorological factors also significantly influence vegetation phenology [39]. Previous studies have defined the preseason length as the period before the multiyear average SOS [40]. The most relevant time periods for flowering and leaf out are typically the previous one to three months before the phenological event [41]. Based on multiyear phenological values, SOS mostly occurs from mid-to-late April to early May, while EOS frequently takes place in October and November. To ensure capturing all the relevant climate change information preceding phenological events [42], we selected a longer preseason time frame, designating January to April as the period affecting SOS and July to October as the period influencing EOS. Regarding the time of urbanization impact factors, since urbanization is typically calculated annually, we considered it on an annual basis. Table I presents the explanatory variables and factor codes for each model. Before modeling, a diagnosis of covariance was performed to address potential multicollinearity among the variables. The variance inflation factor (VIF) was utilized to assess the covariance, and variables with VIF values exceeding 10 were excluded from consideration. Specifically, in the SOS model, explanatory variables X1, X4, X5, X6, X7, X8, and X9 were retained, while in the EOS model, explanatory variables X1, X2, X3, X4, X5, X6, X7, X8, and X9 were retained.

4) Evaluation of Model Predictions: In this study, the leave-one-out cross validation was employed to assess the predictive ability of the model. Leave-one-out cross-validation generates independent error estimates for small sample datasets that cannot be divided into training sets and testing sets. For a dataset with n observations, the best fitting GAM uses $n - 1$ points in each iteration and predicts the remaining point, resulting in n fits. After n iterations, error statistics can be generated

TABLE I
EACH PREDICTOR AND FACTOR CODE

Phenological Parameter	Influencing Factor	Explanatory Variable	Implication	Values
SOS	Climate change	X1	Accumulated precipitation	1.930
		X2	Mean minimum temperature	12.739
		X3	Mean maximum temperature	26.294
		X4	Accumulated sunshine hours	4.334
		X5	Mean wind speed	7.433
		X6	Mean humidity	3.778
	Urbanization	X7	Urban heat island intensity	5.274
		X8	Nighttime light intensity	2.114
		X9	Population density	4.648
EOS	Climate change	X1	Accumulated precipitation	5.763
		X2	Mean minimum temperature	7.121
		X3	Mean maximum temperature	6.526
		X4	Accumulated sunshine hours	4.011
		X5	Mean wind speed	4.557
		X6	Mean humidity	3.848
	Urbanization	X7	Urban heat island intensity	1.565
		X8	Nighttime light intensity	2.037
		X9	Population density	7.364

The meteorological data from january to april of 2001 to 2020 are selected as the meteorological explanatory variables of SOS, and the data from july to october of 2001 to 2020 are selected as the meteorological explanatory variables of EOS. The annual average change from 2001 to 2020 is selected as the explanatory variable for urbanization.

from n individual residuals. Root-mean-square error (RMSE) and coefficient of determination (R^2) were used to evaluate the predictive ability of the model

$$R^2 = 1 - \frac{\sum_{i=1}^{n}(y_i - \hat{y}_i)^2}{\sum_{i=1}^{n}(y_i - \bar{y})^2} \tag{4}$$

$$\text{RMSE} = \sqrt{\frac{1}{n}\sum_{i=1}^{n}(y_i - \hat{y}_i)^2} \tag{5}$$

where n is the number of observations, y_i is the observed data, $\hat{y}_i$ is the predicted data, and $\bar{y}_i$ is the average of the observed data.

IV. RESULTS

A. Extraction Results of Vegetation Phenological Parameters

The phenological parameters SOS and EOS extracted by the D-L function method and the dynamic threshold method were verified with the start and end of the vegetation growth season in MCD12Q2, respectively. Among all SOS pixels, 64.2% were earlier than the SOS from MCD12Q2 and 35.8% were later, with an average difference of 1.92 days [see Fig. 3(a)]. Larger differences were primarily observed in urban areas. Across all EOS pixels, 91.5% were ahead of the EOS of MCD12Q2, while 8.5% lagged behind, with an average difference of 9.00 days [see Fig. 3(b)]. There was a significant correlation between SOS and the SOS obtained from MCD12Q2 ($r = 0.865$, $p < 0.01$, and RMSE = 4.529 days) [see Fig. 3(c)]. Similarly, there was a significant correlation between EOS and the EOS obtained from MCD12Q2 ($r = 0.771$, $p < 0.01$, and RMSE = 4.918 days) [see Fig. 3(d)]. Overall, the comparison with the MCD12Q2 data validated the accuracy of the extracted phenological parameters, which can be used for further analysis of the spatiotemporal characteristics of vegetation phenology.

B. Temporal and Spatial Characteristics of Vegetation Phenology

Based on the D-L fitting method and the dynamic threshold value extraction method, the annual average distribution of SOS and EOS in Beijing from 2001 to 2020 was obtained (see Fig. 4). There were overall spatial differences in the vegetation phenology distribution between the southeast and northwest regions. From 2001 to 2020, SOS in Beijing was mostly concentrated within the range of 110–125 days. SOS occurred earlier in the southeast, and the overall distribution feature was that SOS was delayed from southeast to northwest. EOS was mostly concentrated within the range of 290–300 days, with a distribution pattern similar to SOS. In addition, the southwest and northern regions exhibited an earlier end of phenology, with the end of phenology gradually advancing from the southeast to the northwest. SOS occurred earlier in urban areas compared to

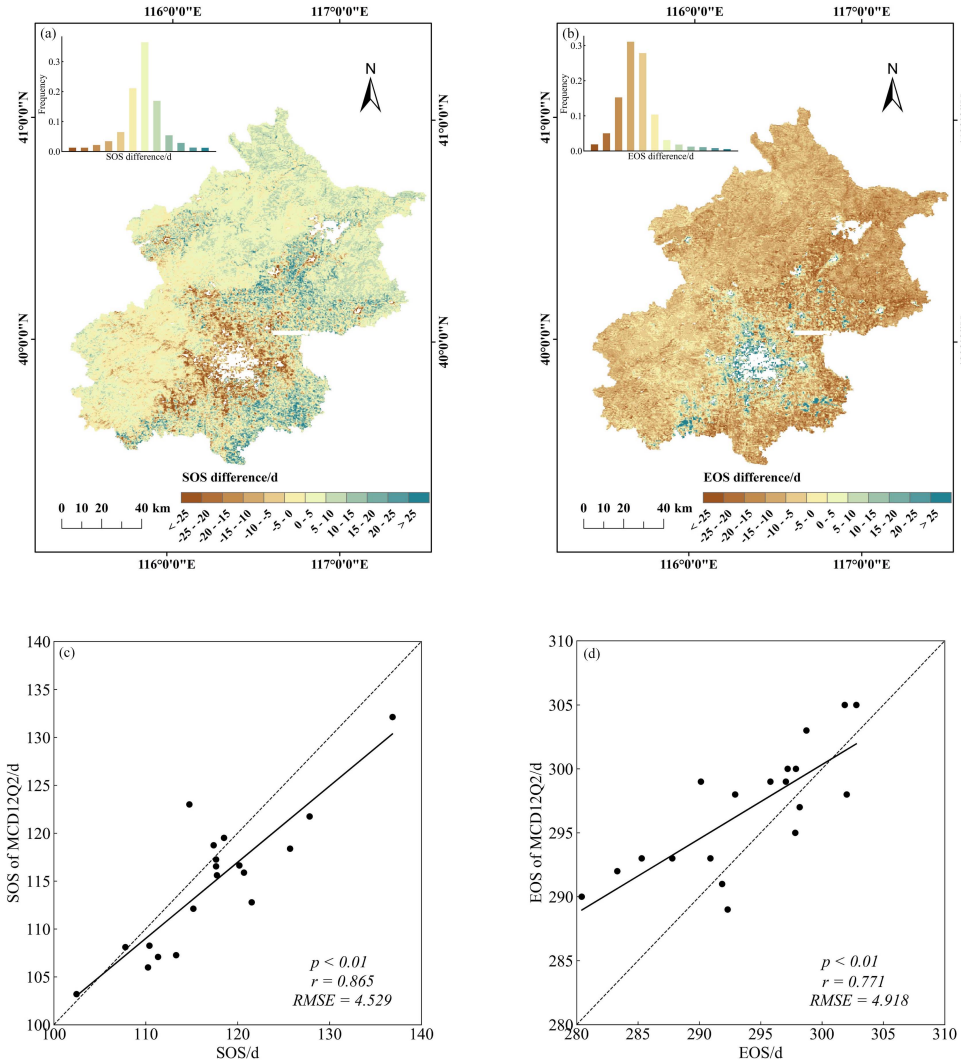

Fig. 3. Phenological parameter validation on temporal and spatial levels. Spatial comparison of (a) SOS and SOS of MCD12Q2 and (b) EOS and EOS of MCD12Q2. Temporal relationship between (c) SOS and SOS of MCD12Q2 and (d) EOS and EOS of MCD12Q2. The solid black line denotes the linear regression line.

surrounding areas, while EOS occurred later. Moreover, as the distance from the urban areas increased, the SOS occurred later, and the EOS occurred earlier.

Significant phenological changes were observed in Beijing from 2001 to 2020, with an overall trend of advanced SOS and delayed EOS (see Fig. 5). The fitted curve slopes indicated that SOS advanced at a rate of 0.850 day/year ($p < 0.01$) and EOS was delayed at a rate of 0.918 day/year ($p < 0.01$). The SOS ranged from 102.5 to 136.9 days in Beijing, with an average of 117.2 days. The earliest SOS was observed in 2017, lasting less than 110 days, while the latest SOS occurred in 2006, lasting over 130 days. The EOS ranged from 280.4 to 302.8 days, with an average of 293.9 days. The earliest EOS appeared in 2002, around 280 days, while the latest EOS occurred in 2019, exceeding 300 days.

There were significant phenological changes in Beijing, particularly in urban, suburban, and rural areas. Urban areas exhibited an earlier SOS and a later EOS (see Fig. 6). Conversely, rural areas exhibited the latest SOS and the earliest EOS. SOS in urban areas advanced on average by 0.50 day/year ($p < 0.05$) [see Fig. 6(a)], while both suburban and rural areas exhibited consistent trends of SOS advancement, averaging 0.96 day ($p < 0.01$) and 0.64 day/year ($p < 0.05$), respectively. EOS in suburban and rural areas were significantly delayed, with average delays of 0.97 and 0.94 day/year ($p < 0.01$), respectively. Compared with suburban and rural areas, urban areas demonstrated a more stable EOS, with an average delay of 0.76 day/year ($p < 0.01$) [see Fig. 6(b)].

C. Relationships Between Meteorological, Urban Factors, and Vegetation Phenological Parameters

1) GAM Fitting Results of SOS: In the single-factor GAM, nighttime light intensity and population density had a significant impact on the dependent variable at the $p < 0.01$ level, as shown in Table II. This indicated that nighttime light intensity and population density were both statistically significant when used individually as explanatory variables for SOS variations. The

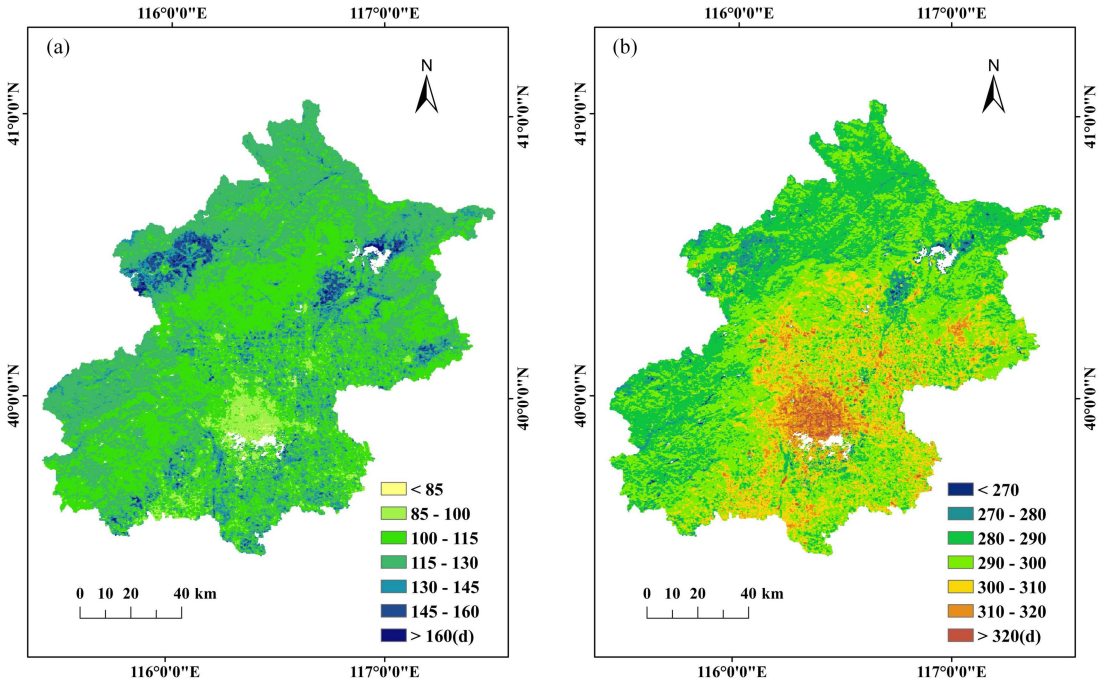

Fig. 4. Annual vegetation phenological parameters (a) SOS and (b) EOS in Beijing from 2001 to 2020.

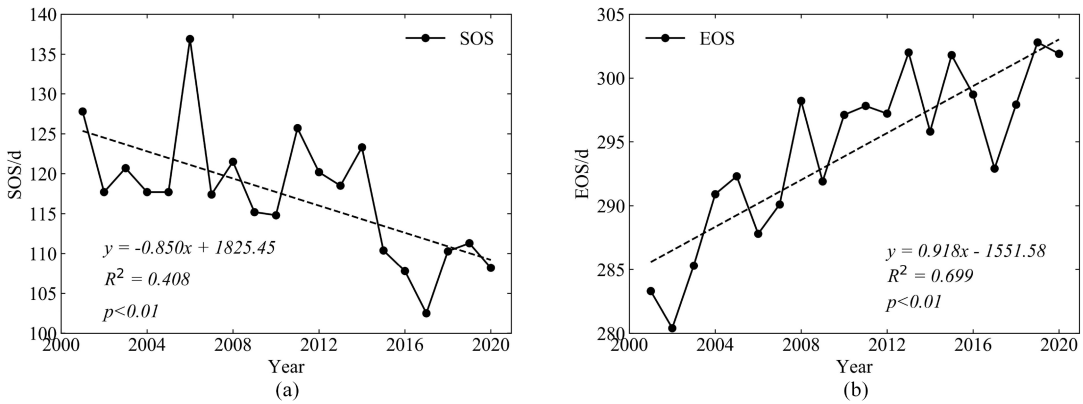

Fig. 5. Interannual variations of (a) SOS and (b) EOS from 2001 to 2020 in Beijing. The dashed black line denotes the linear regression line.

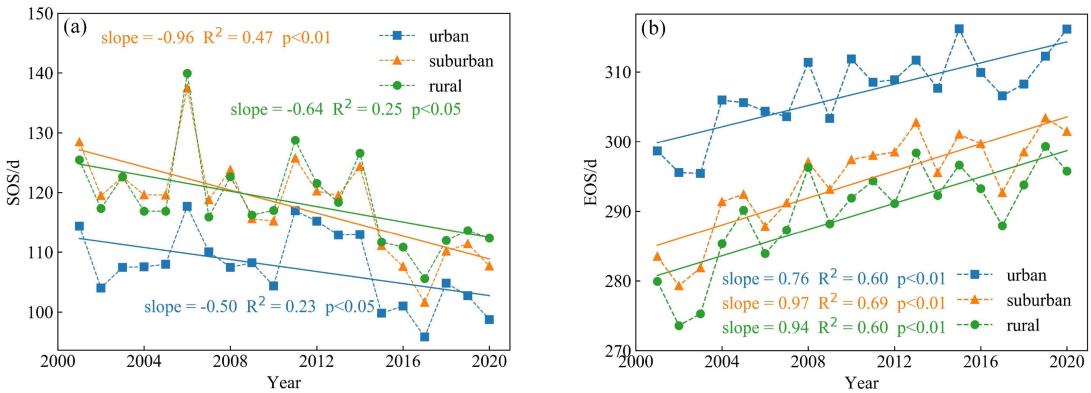

Fig. 6. Interannual variations of (a) SOS and (b) EOS in urban, suburban, and rural areas from 2001 to 2020. Suburban is the combination of all buffer zones between 0 and 20 km from the edge of the urban. The slope value refers to the slope of the linear regression line.

TABLE II
SINGLE-FACTOR GAM FITTING RESULTS OF SOS, METEOROLOGICAL FACTORS, AND URBANIZATION FACTORS

Independent Variable	Edf	Ref. df	*F* value	*p*-value	Adjusted R^2	Deviance explained
X1 Accumulated precipitation	4.877	5.896	1.68	0.181	0.301	48.1%
X4 Accumulated sunshine hours	5.48	6.589	1.797	0.169	0.336	52.8%
X5 Mean wind speed	1	1	2.831	0.11	0.0879	13.6%
X6 Mean humidity	1	1	0.005	0.943	—0.0552	0.0296%
X7 Urban heat island intensity	1.464	1.799	1.156	0.249	0.0955	16.5%
X8 Nighttime light intensity	7.996	8.739	5.346	0.0051**	0.669	82.6%
X9 Population density	1	1	17.15	0.000612***	0.459	48.8%

Note: Edf is the estimated degree of freedom; Ref. df is the reference degree of freedom.
* indicates significant contribution at the 0.05 level, ** indicates significant contribution at the 0.01 level, *** indicates significant contribution at the 0.001 level.

TABLE III
SINGLE-FACTOR GAM FITTING RESULTS OF EOS, METEOROLOGICAL FACTORS, AND URBANIZATION FACTORS

Independent Variable	Edf	Ref. df	*F* value	*p*-value	Adjusted R^2	Deviance explained
X1 Accumulated precipitation	1.877	2.345	5.471	0.013*	0.384	44.5%
X2 Mean minimum temperature	1.727	2.154	0.545	0.541	0.0326	12.1%
X3 Mean maximum temperature	6.248	7.288	5.06	0.00604**	0.635	75.5%
X4 Accumulated sunshine hours	1	1	0.001	0.976	-0.0555	0.00526%
X5 Mean wind speed	1.843	2.31	15.39	0.000115***	0.645	67.9%
X6 Mean humidity	1.098	1.19	0.023	0.97	-0.0492	1.15%
X7 Urban heat island intensity	1	1	0.045	0.834	-0.0529	0.251%
X8 Nighttime light intensity	2.012	2.499	2.343	0.0977	0.23	31.2%
X9 Population density	2.667	3.33	18.5	1.66e-05***	0.762	79.5%

Note: Edf is the estimated degree of freedom; Ref. df is the reference degree of freedom.
* indicates significant contribution at the 0.05 level, ** indicates significant contribution at the 0.01 level, *** indicates significant contribution at the 0.001 level.

deviance explained by nighttime light intensity and population density was greater than 40%, with nighttime light intensity explaining 82.6% of the deviance. Among all the factors affecting SOS changes, mean wind speed, mean humidity, and population density exhibited linear relationships with SOS changes, while accumulated precipitation, accumulated sunshine hours, urban heat island intensity, and nighttime light intensity showed nonlinear relationships with SOS changes. Among these, the nonlinear relationship between nighttime light intensity and SOS was the strongest. SOS changes are complex nonlinear changes affected by multiple factors. Therefore, the GAM can be used to analyze the nonlinear relationships between multiple independent variables and the SOS-dependent variable.

By analyzing all possible models, the optimal model was determined based on the deviance explained and the minimum AIC value. The final expression of the SOS model is as follows:

Model SOS: s (SOS) = s (nighttime light intensity) + s (accumulated sunshine hours) + s (accumulated precipitation) + mean wind speed + population density, the accumulated interpretation of SOS in Beijing reached 68.1%.

2) GAM Fitting Results of EOS: In the single-factor GAM, accumulated precipitation, mean maximum temperature, mean wind speed, and population density had a significant impact on the dependent variable at the $p < 0.05$ level, as shown in Table III. This indicated that the above four factors were all statistically significant when used as explanatory variables for EOS changes alone, with population density explaining 79.5% of the deviance. Among all factors affecting EOS changes, accumulated precipitation, mean minimum temperature, mean maximum temperature, mean wind speed, mean humidity, nighttime light intensity, and population density all exhibited nonlinear relationships with EOS changes. Notably, the nonlinear relationship between mean maximum temperature and EOS was found to be the strongest. In addition, there were linear relationships between accumulated sunshine hours, urban heat island intensity, and EOS.

By analyzing all possible models, the optimal model was determined based on the deviance explained and the minimum AIC value. The final expression of the EOS model is as follows:

Model EOS: s (EOS) = s (population density) + s (mean wind speed) + s (mean humidity) + urban heat island intensity, the accumulated interpretation of EOS in Beijing reached 73.9%.

D. Prediction Results of Vegetation Phenological Parameters

1) Prediction of Vegetation Phenological Parameters: Based on the above models, the predictive performance of SOS and EOS across the urban–rural gradient was evaluated using a leave-one-out cross-validation method. According to the principle of leave-one-out cross-validation, the 19-year phenological parameters were selected as the training set each time, with the remaining one-year phenological parameters used as the test set. This entire process was repeated 20 times, and the optimal model was chosen for vegetation phenology simulation and prediction.

Fig. 7(a) presents the comparison between the observed and predicted values of SOS, showing an R^2 of 0.622 between the observed and predicted values of SOS ($p < 0.01$), with an RMSE of 4.654 days. Fig. 7(b) illustrates the comparison between the observed and predicted values of EOS, revealing an R^2 of 0.756

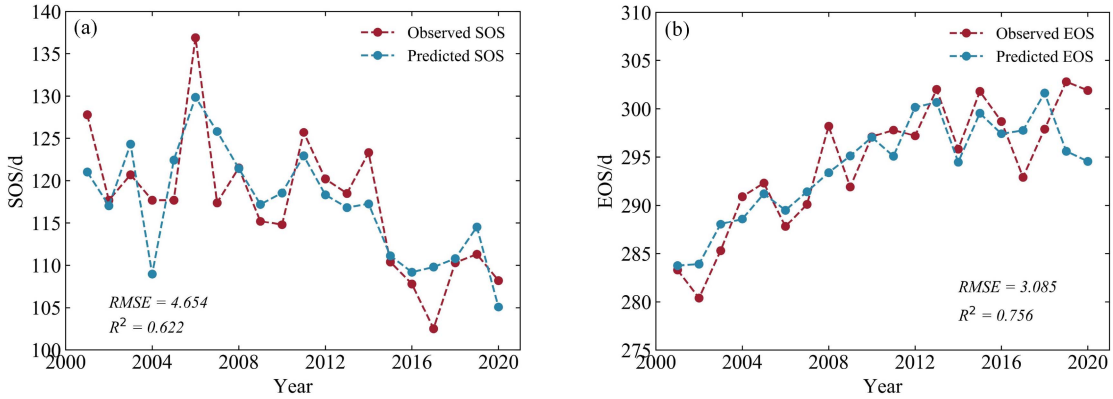

Fig. 7. Comparison of predicted and observed values of SOS and EOS.

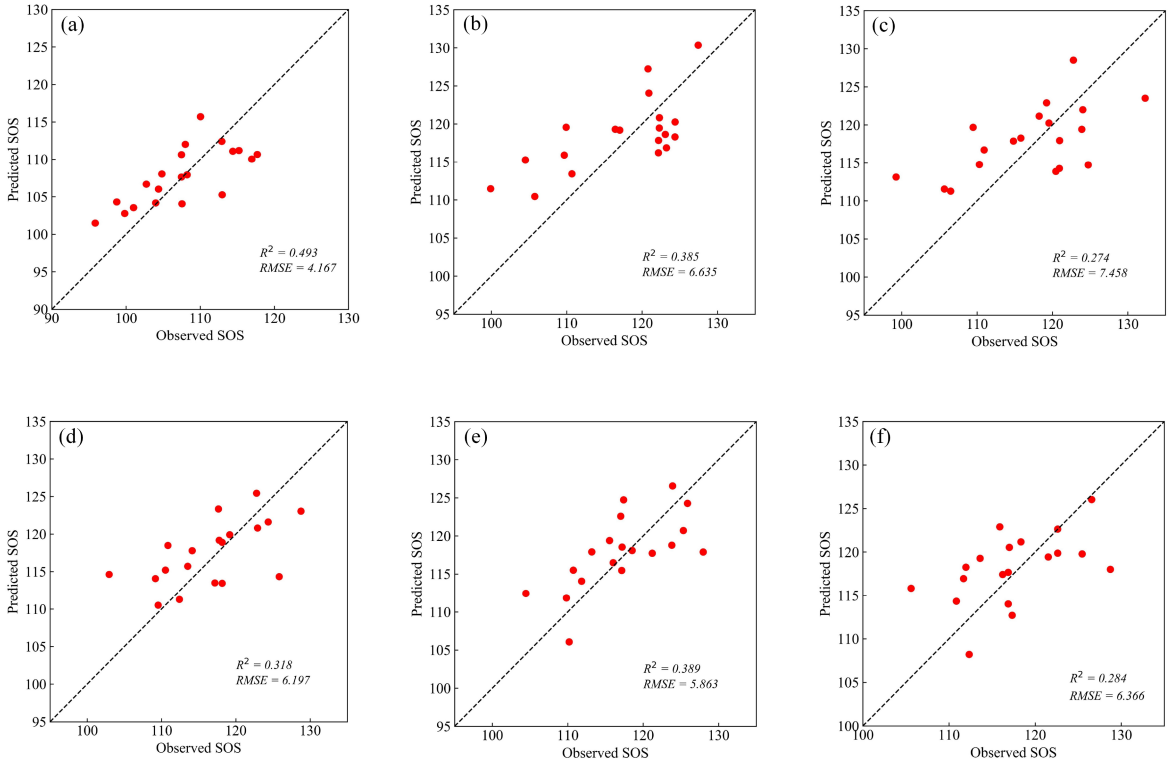

Fig. 8. Prediction results of SOS across different urban–rural gradient zones. (a) Urban. (b) 0–5 km buffer zone. (c) 5–10 km buffer zone. (d) 10–15 km buffer zone. (e) 15–20 km buffer zone. (f) Rural.

between the observed and predicted values of EOS ($p < 0.01$), with an RMSE of 3.085 days. Both models performed well and can predict vegetation phenology in Beijing effectively.

2) Prediction of Vegetation Phenological Parameters Along the Urban–Rural Gradient: Along the urban–rural gradient, the SOS and EOS were predicted for different regions of Beijing. Fig. 8 illustrates the SOS prediction results, which showed satisfactory predictions in various regions along the urban–rural gradient, with R^2 ranging from 0.274 to 0.493 and RMSE between 4.167 and 7.458 days. The EOS predictions across different urban–rural gradient zones (see Fig. 9) also exhibited good performance, with R^2 between 0.166 and 0.650 and RMSE ranging from 4.177 to 6.537 days. Through a comparative analysis of the SOS and EOS predictions in different regions along the urban–rural gradient, the accuracy of predicting SOS and EOS in areas with varying degrees of urbanization through GAM was validated.

V. Discussion

Analyzing the relationship between vegetation phenology and the external environment is an ongoing field of research [33], [43], [44], [45]. Previous studies have primarily relied on simple statistical relationships between phenology and external factors [46], [47]. However, the actual response of vegetation phenology to external environmental changes is complex and

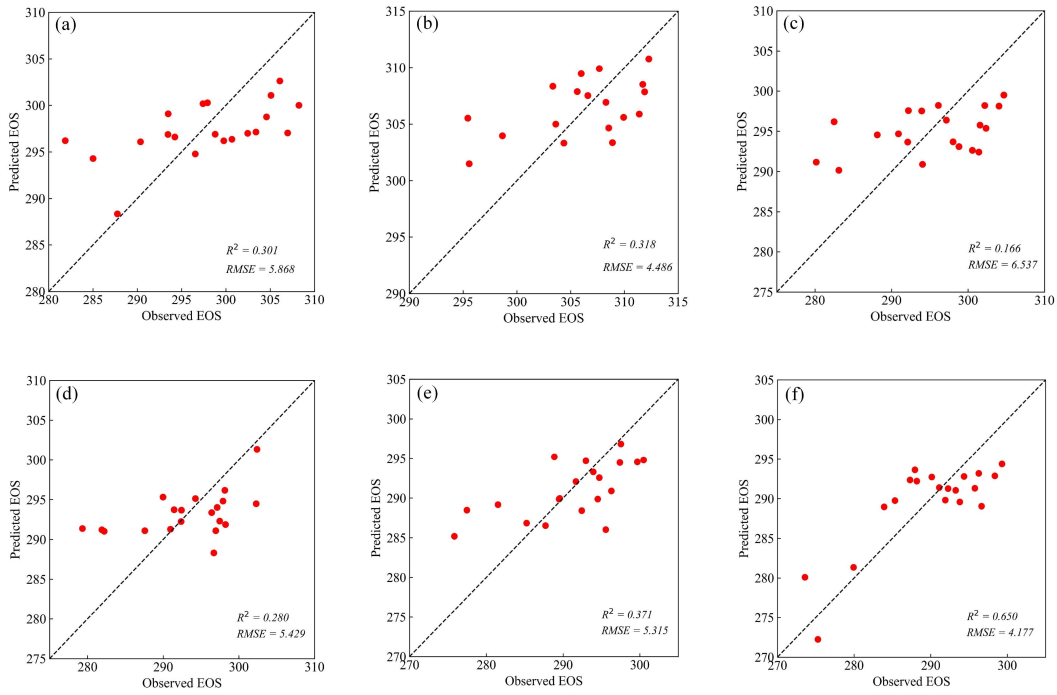

Fig. 9. Prediction results of EOS across different urban–rural gradient zones. (a) Urban. (b) 0–5 km buffer zone. (c) 5–10 km buffer zone. (d) 10–15 km buffer zone. (e) 15–20 km buffer zone. (f) Rural.

nonlinear [48], [49]. This study utilized the GAM to investigate the influencing factors of vegetation phenology and analyze the relationships between climate change, urbanization, and vegetation phenology. The findings suggested that vegetation phenology exhibited heterogeneity both temporally and spatially. Through GAM analysis, it was found that the responses of SOS and EOS to climate change and urbanization were nonlinear. The feasibility of GAM in predicting phenology was verified by predicting vegetation phenology across different urban–rural gradient zones. The GAM quantitatively analyzed the impact of climate change and urbanization on vegetation phenology. This methodology can provide insights for future phenology predictions.

A. *Vegetation Phenological Parameters*

In this study, vegetation phenological parameters were extracted using the D-L function method and the dynamic threshold method based on MODIS data. While MODIS data are widely used in vegetation phenology parameter extraction [1], [50], it is important to note that phenology assessment based on remote sensing data represents an approximation of real vegetation phenology and entails a certain degree of uncertainty [16]. The extraction of vegetation phenological parameters from remote sensing data using smoothing algorithms and dynamic threshold methods is somewhat subjective, which may introduce biases into the phenological extraction results. In order to verify the accuracy of the extraction results, many researchers have chosen to compare the extracted results with physical measurements of vegetation phenology from different satellite products [50], [51]. The correlation between the extracted phenological parameters and the phenological information obtained from MCD12Q2 data was greater than 0.7 (see Fig. 3), which verified the accuracy of the results to a certain extent. However, in future research, it is still necessary to consider the use of higher resolution data and incorporate the vegetation growth curve change pattern for phenological parameter extraction. Researchers have explored the harmonized Landsat 8 and Sentinel-2 (HLS), which can be used to estimate the time of vegetation phenology at a spatial resolution of 30 m [52], [53]. Overall, from 2001 to 2020, there were significant spatiotemporal changes in vegetation phenology in Beijing. The spatial distribution of vegetation phenology in Beijing differed between the southeast and northwest (see Fig. 4), which is considered to be influenced by the high northwest and low southeast topography of Beijing. The city as a whole showed an early SOS and a delayed EOS (see Fig. 5), consistent with findings observed by other researchers in urban phenology studies [50], [54].

B. *Model Construction Factors Selection*

Meteorological factors are the primary environmental factors that affect vegetation phenology. Temperature plays a crucial role in vegetation growth and development. Vegetation needs low temperature to induce chilling before breaking the physiological dormancy and entering the ecological dormancy period, while high temperature promotes the transition of vegetation from ecological dormancy to the growth period [55]. Warming in winter can reduce the accumulation of low temperature received by plants during the dormant period, thereby increasing the accumulated temperature demand of plants in spring, which has a delayed effect on spring phenology [10]. Precipitation is an essential water source for vegetation growth and development,

and plants grow and develop faster when there is sufficient moisture. The increase of water promotes the early greening period, while the warm and humid autumn is conducive to the delay of the yellowing period [56]. In recent years, temperature and precipitation have been widely recognized as key limiting factors for vegetation growth and strong drivers of phenological events. However, the start and end of the phenological period are not always dependent on temperature and precipitation. Wind speed also affect vegetation evapotranspiration. It can accelerate the dissipation of soil moisture at the surface interface, affecting vegetation growth. In addition, the weakening of the wind speed can cause leaf shedding, reducing cooling effect and frost damage, and slowing leaf senescence [57]. For vegetation in Beijing, there was a relatively high chance of vegetation entering the end of the growth period being influenced by mean wind speed (see Table III). Photoperiod promotes leaf germination in plants. Many plants require a certain duration of sunshine after the end of the spring dormancy period to initiate new leaf growth. The likelihood of vegetation starting to grow and develop was relatively high under conditions of sufficient sunshine (see Table II). Photoperiod regulates vegetation phenology by delaying leaf expansion caused by temperature changes, thereby reducing the risk of leaves suffering from frost [58]. Humidity is an important factor that affects plant transpiration and also affects vegetation growth and development. Some scholars believe that humidity is a more stable climate signal than temperature and precipitation [59]. Higher humidity can be accompanied by lower temperature and a higher risk of frost. Therefore, as humidity rises, trees may delay leaf unfolding to prevent frost [60]. In the process of urbanization, human activities cannot be ignored. Urban areas with high population densities typically have more buildings, impermeable surfaces, and traffic activities, leading to higher temperature compared to surrounding areas [8]. The higher temperature in urban environments enhances plant transpiration, accelerates water evaporation rates, and results in soil dryness and water scarcity, ultimately leading to an earlier onset of vegetation phenology. Nighttime light intensity refers to the visible and near-infrared electromagnetic wave information emitted from the surface under cloudless conditions at night. It can serve as an effective representation of human activities and is widely used in urbanization processes and ecological assessments [61]. Nighttime light intensity accelerates the bud break process and delays leaf coloring. With the process of urbanization, nighttime light intensity will have more complex effects on terrestrial ecosystems [62]. As an important indicator of terrestrial ecosystems, vegetation phenology exhibits a strong response to nighttime light intensity. Nighttime light intensity explained 82.6% of the deviance in SOS and 31.2% of the deviance in EOS (see Tables II and III). This indicates a strong response of vegetation phenology to nighttime light intensity and further emphasizes the significant impact of urbanization on vegetation growth and development. Therefore, when constructing a GAM to predict vegetation phenology, it is important to consider these influencing factors comprehensively for a better analysis of vegetation phenological changes.

C. Performance of GAM

According to previous studies, climate change is the most significant factor affecting vegetation phenology [3]. Specifically, most studies only consider a linear relationship between climate change and vegetation phenology [15]. However, with the rapid development of urbanization, urbanization is also considered as potential factor that has a significant impact on vegetation phenology prediction [63], [64]. In this study, the GAM was employed to explore the relationships between vegetation phenology, climate change, and urbanization, based on smooth functions of each explanatory variable. The best models were determined based on the deviance explained and the lowest AIC value. When using nighttime light intensity + accumulated sunshine hours + accumulated precipitation + mean wind speed + population density, the SOS model showed the best results with the lowest AIC value. When using population density + mean wind speed + mean humidity + urban heat island intensity, the EOS model showed the best results with the lowest AIC value. The study showed that the response of vegetation phenology to external factors is a highly complex process, rather than a simple linear relationship, which is consistent with the conclusions from other researchers [65], [66]. The RMSE between the predicted and observed vegetation phenology values was approximately 4–7 days, showing a comparable accuracy to other results on the predicted phenology [49], [67]. Specifically, the method proposed in this study took into account the combined effects of climate change and urbanization on vegetation phenology and could be expected to be better applied to vegetation phenology prediction in urban areas. Our results can contribute to understanding the impact of climate change and urbanization on vegetation phenology and provide important information for ecological conservation and restoration.

The GAM performed well and predicted vegetation phenological parameters with small errors. However, significant prediction errors still exist in certain years. In addition to climate change and urbanization, vegetation phenology may also be affected by other external factors, such as soil conditions and water resources [68]. These factors were not considered in this study, which could lead to prediction errors and biases. The basic assumption of the GAM is that the relationships between variables are additive, meaning that the effects of variables are independent and can be simply added together to obtain the overall effect [11]. However, the relationships between phenology, climate change, and urbanization may not be simply additive, and there may be complex interactions and nonlinear relationships. Further research and analysis are still needed for these complex interactions. In general, future research can explore the integration of GAM with data from different scales and sources [28]. In addition, considering the integration of GAM with other prediction methods and models can improve the capability and interpretability of phenology predictions.

VI. Conclusion

This study revealed the spatiotemporal distributional characteristics of vegetation phenological parameters in Beijing. Vegetation phenology exhibited spatial variations between the

southeast and northwest regions, with an earlier onset of SOS and a delayed onset of EOS as the overall trend. By considering vegetation phenological parameters as response variables and with meteorological and urbanization factors as explanatory variables, the GAM was constructed to explore the response of vegetation phenology to climate change and urbanization and predict its phenological patterns. The findings demonstrated that the changes in SOS and EOS were the combined effects of climate change and urbanization. SOS showed a nonlinear advancement in response to accumulated precipitation, accumulated sunshine hours, urban heat island intensity, and nighttime light intensity. EOS exhibited a nonlinear delay in response to accumulated precipitation, mean minimum temperature, mean maximum temperature, mean wind speed, mean humidity, nighttime light intensity, and population density. Nighttime light intensity and population density played a dominant role in vegetation phenological changes, further emphasizing the significant impact of urbanization. The GAM significantly improved the performance of phenology predictions, with RMSE of approximately 4–7 days. In conclusion, the GAM has been proven to be a valuable tool for analyzing the nonlinear relationships between vegetation phenology and external environmental changes, with potential applications in phenology analysis and prediction.

REFERENCES

[1] L. Li et al., "Detection and attribution of long-term and fine-scale changes in spring phenology over urban areas: A case study in New York state," *Int. J. Appl. Earth Observ. Geoinf.*, vol. 110, 2022, Art. no. 102815.

[2] Y. S. Christopher, P. Wong, D'Y. Odorico, M. Bhathena, A. Arain, and I. Ensminger, "Carotenoid based vegetation indices for accurate monitoring of the phenology of photosynthesis at the leaf-scale in deciduous and evergreen trees," *Remote Sens. Environ.*, vol. 233, 2019, Art. no. 111407.

[3] P. Ren et al., "Strong controls of daily minimum temperature on the autumn photosynthetic phenology of subtropical vegetation in China," *Forest Ecosyst.*, vol. 8, no. 1, 2021, Art. no. 31.

[4] J. Penuelas and I. Filella, "Phenology. Responses to a warming world," *Science*, vol. 294, no. 5543, pp. 793–795, 2001.

[5] J. Tang et al., "Emerging opportunities and challenges in phenology: A review," *Ecosphere*, vol. 7, no. 8, 2016, Art. no. e01436.

[6] S. Wang et al., "Urban-rural gradients reveal joint control of elevated $CO(_2)$ and temperature on extended photosynthetic seasons," *Nature Ecol. Evol.*, vol. 3, no. 7, pp. 1076–1085, 2019.

[7] D. Zhou, S. Zhao, L. Zhang, G. Sun, and Y. Liu, "The footprint of urban heat island effect in China," *Sci. Rep.*, vol. 5, no. 1, 2015, Art. no. 11160.

[8] D. Li, B. J. Stucky, J. Deck, B. Baiser, and R. P. Guralnick, "The effect of urbanization on plant phenology depends on regional temperature," *Nature Ecol. Evol.*, vol. 3, no. 12, pp. 1661–1667, 2019.

[9] D. Zhou, S. Zhao, L. Zhang, and S. Liu, "Remotely sensed assessment of urbanization effects on vegetation phenology in China's 32 major cities," *Remote Sens. Environ.*, vol. 176, pp. 272–281, 2016.

[10] X. Wang, P. Du, D. Chen, C. Lin, H. Zheng, and S. Guo, "Characterizing urbanization-induced land surface phenology change from time-series remotely sensed images at fine spatio-temporal scale: A case study in Nanjing, China (2001–2018)," *J. Cleaner Prod.*, vol. 274, 2020, Art. no. 122487.

[11] Q. Huang, L. Peng, K. Huang, W. Deng, and Y. Liu, "Generalized additive model reveals nonlinear trade-offs/synergies between relationships of ecosystem services for mountainous areas of Southwest China," *Remote Sens.*, vol. 14, no. 12, 2022, Art. no. 2733.

[12] A. M. Iler, T. T. Hoye, D. W. Inouye, and N. M. Schmidt, "Nonlinear flowering responses to climate: Are species approaching their limits of phenological change?," *Philos. Trans. Roy. Soc. London B, Biol. Sci.*, vol. 368, no. 1624, 2013, Art. no. 20120489.

[13] B. R. Lee et al., "Wildflower phenological escape differs by continent and spring temperature," *Nature Commun.*, vol. 13, no. 1, 2022, Art. no. 7157.

[14] K. S. Pope, V. Dose, D. Da Silva, P. H. Brown, C. A. Leslie, and T. M. Dejong, "Detecting nonlinear response of spring phenology to climate change by Bayesian analysis," *Glob. Change Biol.*, vol. 19, no. 5, pp. 1518–25, 2013.

[15] T. Zhou, R. Cao, S. Wang, J. Chen, and Y. Tang, "Responses of green-up dates of grasslands in China and woody plants in Europe to air temperature and precipitation: Empirical evidences based on survival analysis," *Chin. J. Plant Ecol.*, vol. 42, no. 5, pp. 526–538, 2018.

[16] O. Celis-Hernandez, M. Villoslada-Pecina, R. D. Ward, T. F. Bergamo, R. Perez-Ceballos, and M. P. Giron-Garcia, "Impacts of environmental pollution on mangrove phenology: Combining remotely sensed data and generalized additive models," *Sci. Total Environ.*, vol. 810, 2022, Art. no. 152309.

[17] H. F. Evans and J. Shen, "Long-term hindcasts of wheat yield in fields using remotely sensed phenology, climate data and machine learning," *Remote Sens.*, vol. 13, no. 13, 2021, Art. no. 2435.

[18] A. Guisan, Thomas C. Edwards, and T. Hastie, "Generalized linear and generalized additive models in studies of species distributions: Setting the scene," *Ecol. Model.*, vol. 157, no. 2, pp. 89–100, 2002.

[19] X. Chen, P. Xue, L. Liu, L. Gao, and J. Liu, "Outdoor thermal comfort and adaptation in severe cold area: A longitudinal survey in Harbin," *China. Building Environ.*, vol. 143, pp. 548–560, 2018.

[20] B. Georges, A. Michez, N. Latte, P. Lejeune, and Y. Brostaux, "Water stream heating dynamics around extreme temperature events: An innovative method combining gam and differential equations," *J. Hydrol.*, vol. 601, 2021, Art. no. 126600.

[21] S. Suárez-Seoane, Patrick E. Osborne, and J. C. Alonso, "Large-scale habitat selection by agricultural steppe birds in Spain: Identifying species-habitat responses using generalized additive models," *J. Appl. Ecol.*, vol. 39, no. 5, pp. 755–771, 2002.

[22] B. de Foy, M. G. Saroar, A. Salam, and J. J. Schauer, "Distinguishing air pollution due to stagnation, local emissions, and long-range transport using a generalized additive model to analyze hourly monitoring data," *ACS Earth Space Chem.*, vol. 5, no. 9, pp. 2329–2340, 2021.

[23] G. Yuan, S. Weixuan, and Y. Yongtao, "Air pollution and coronary heart disease-related hospital visits in Beijing, China: Time-series analysis using a generalized additive model," *Environ. Sci. Pollut. Res. Int.*, vol. 30, no. 13, pp. 36938–36951, 2022.

[24] Á. S. Esther et al., "Placental levels of essential and non-essential trace element in relation to neonatal weight in northwestern Spain: Application of generalized additive models," *Environ. Sci. Pollut. Res. Int.*, vol. 30, no. 22, pp. 62566–62578, 2023.

[25] J. Jbilou and S. El Adlouni, *Generalized Additive Models in Environmental Health: A Literature Review*. London, U.K.: IntechOpen, 2012.

[26] M. A. White, R. R. Nemani, P. E. Thornton, and S. W. Running, "Satellite evidence of phenological differences between urbanized and rural areas of the eastern United States deciduous broadleaf forest," *Ecosystems*, vol. 5, no. 3, pp. 260–273, 2002.

[27] C. Song and M. Cao, "Relationships between plant species richness and terrain in middle sub-tropical eastern China," *Forests*, vol. 8, 2017, Art. no. 344.

[28] N. Younes, T. D. Northfield, K. E. Joyce, S. W. Maier, N. C. Duke, and L. Lymburner, "A novel approach to modelling mangrove phenology from satellite images: A case study from northern Australia," *Remote Sens.*, vol. 12, no. 24, 2020, Art. no. 4008.

[29] Y. Zhang et al., "The divergent response of vegetation phenology to urbanization: A case study of Beijing city, China," *Sci. Total Environ.*, vol. 803, 2022, Art. no. 150079.

[30] C. He, Z. Liu, W. Lu, and M. Xu, "Dataset of urban built-up area in China (1992–2020) v1.0," National Tibetan Plateau Data Center, 2022.

[31] X. Li, C. Zhang, and D. Meng, "Spatial and temporal changes of vegetation phenology and its response to urbanization in the Beijing-Tianjin-Hebei region," *Acta Ecol. Sinica*, vol. 43, pp. 249–262, 2023.

[32] Z. Chen et al., "An extended time series (2000–2018) of global NPP-VIIRS-like nighttime light data from a cross-sensor calibration," *Earth Syst. Sci. Data*, vol. 13, pp. 889–906, 2020.

[33] Z. Liu, Y. Zhou, and Z. Feng, "Response of vegetation phenology to urbanization in urban agglomeration areas: A dynamic urban-rural gradient perspective," *Sci. Total Environ.*, vol. 864, 2023, Art. no. 161109.

[34] M. Shen et al., "Can changes in autumn phenology facilitate earlier green-up date of northern vegetation?," *Agricultural Forest Meteorol.*, vol. 291, 2020, Art. no. 108077.

[35] G. L. Simpson, "Modelling palaeoecological time series using generalised additive models," *Front. Ecol. Evol.*, vol. 6, 2018, Art. no. 149.

[36] S. E. Jørgensen, *Model Selection and Multimodel Inference: A Practical Information–Theoretic Approach*, 2nd ed., K. P. Brunham and D. R. Anderson. Berlin, Germany: Springer, 2002.
[37] V. Gomez-Rubio, "Generalized additive models: An introduction with R (2nd edition)," *J. Statist. Softw.*, vol. 86, 2018, Art. no. 100502.
[38] D. Bera, N. D. Chatterjee, and S. Bera, "Comparative performance of linear regression, polynomial regression and generalized additive model for canopy cover estimation in the dry deciduous forest of West Bengal," *Remote Sens. Appl. Soc. Environ.*, vol. 22, 2021, Art. no. 100502.
[39] M. Shen, Y. Tang, J. Chen, X. Zhu, and Y. Zheng, "Influences of temperature and precipitation before the growing season on spring phenology in grasslands of the central and eastern Qinghai-Tibetan plateau," *Agricultural Forest Meteorol.*, vol. 151, no. 12, pp. 1711–1722, 2011.
[40] S. Piao et al., "Leaf onset in the northern hemisphere triggered by daytime temperature," *Nature Commun.*, vol. 6, no. 1, 2015, Art. no. 6911.
[41] A. Menzel et al., "European phenological response to climate change matches the warming pattern," *Glob. Change Biol.*, vol. 12, pp. 1969–1976, 2006.
[42] H. Yongshuo et al., "Recent spring phenology shifts in western central Europe based on multiscale observations," *Glob. Ecol. Biogeography*, vol. 23, pp. 1255–1263, 2014.
[43] W. Dai, H. Jin, Y. Zhang, T. Liu, and Z. Zhou, "Detecting temporal changes in the temperature sensitivity of spring phenology with global warming: Application of machine learning in phenological model," *Agricultural Forest Meteorol.*, vol. 279, 2019, Art. no. 107702.
[44] Y. Fu, X. Li, X. Zhou, X. Geng, Y. Guo, and Y. Zhang, "Progress in plant phenology modeling under global climate change," *Sci. China Earth Sci.*, vol. 63, no. 9, pp. 1237–1247, 2020.
[45] M. Shen et al., "Plant phenology changes and drivers on the Qinghai–Tibetan plateau," *Nature Rev. Earth Environ.*, vol. 3, no. 10, pp. 633–651, 2022.
[46] T. Ma and C. Zhou, "Climate-associated changes in spring plant phenology in China," *Int. J. Biometeorol.*, vol. 56, no. 2, pp. 269–75, 2012.
[47] C. Wang, R. Cao, J. Chen, Y. Rao, and Y. Tang, "Temperature sensitivity of spring vegetation phenology correlates to within-spring warming speed over the northern hemisphere," *Ecol. Indicators*, vol. 50, pp. 62–68, 2015.
[48] F. Jiao, H. Liu, X. Xu, H. Gong, and Z. Lin, "Trend evolution of vegetation phenology in China during the period of 1981–2016," *Remote Sens.*, vol. 12, no. 3, 2020, Art. no. 572.
[49] X. Q. Ma et al., "Prediction of vegetation phenology with atmospheric reanalysis over semiarid grasslands in inner Mongolia," *Sci. Total Environ.*, vol. 812, 2022, Art. no. 152462.
[50] J. Yang, X. Luo, C. Jin, X. Xiao, and J. Xia, "Spatiotemporal patterns of vegetation phenology along the urban–rural gradient in Coastal Dalian, China," *Urban Forestry Urban Greening*, vol. 54, 2020, Art. no. 126784.
[51] Y. Ji, J. Jin, W. Zhan, F. Guo, and T. Yan, "Quantification of urban heat island-induced contribution to advance in spring phenology: A case study in Hangzhou, China," *Remote. Sens.*, vol. 13, 2021, Art. no. 3684.
[52] D. K. Bolton, J. M. Gray, E. K. Melaas, M. Moon, L. Eklundh, and M. A. Friedl, "Continental-scale land surface phenology from harmonized Landsat 8 and Sentinel-2 imagery," *Remote Sens. Environ.*, vol. 240, 2020, Art. no. 111685.
[53] Y. Shen, X. Zhang, W. Wang, R. Nemani, Y. Ye, and J. Wang, "Fusing geostationary satellite observations with harmonized Landsat-8 and Sentinel-2 time series for monitoring field-scale land surface phenology," *Remote Sens.*, vol. 13, no. 21, 2021, Art. no. 4465.
[54] S. J. Jeong, H. Park, C. H. Ho, and J. Kim, "Impact of urbanization on spring and autumn phenology of deciduous trees in the Seoul capital area, South Korea," *Int. J. Biometeorol.*, vol. 63, no. 5, pp. 627–637, 2019.
[55] N. Delpierre et al., "Temperate and boreal forest tree phenology: From organ-scale processes to terrestrial ecosystem models," *Ann. Forest Sci.*, vol. 73, no. 1, pp. 5–25, 2016.
[56] G. Wang et al., "Preseason heat requirement and days of precipitation jointly regulate plant phenological variations in Inner Mongolian grassland," *Agricultural Forest Meteorol.*, vol. 314, 2022, Art. no. 108783.
[57] C. Wu et al., "Widespread decline in winds delayed autumn foliar senescence over high latitudes," *Proc. Nat. Acad. Sci. USA*, vol. 118, no. 16, 2021, Art. no. e2015821118.
[58] L. Meng et al., "Photoperiod decelerates the advance of spring phenology of six deciduous tree species under climate warming," *Glob. Change Biol.*, vol. 27, no. 12, pp. 2914–2927, 2021.
[59] X. He et al., "Delaying effect of humidity on leaf unfolding in Europe," *Sci. Total Environ.*, vol. 800, 2021, Art. no. 149563.
[60] L. Zipf and R. B. Primack, "Humidity does not appear to trigger leaf out in woody plants," *Int. J. Biometeorol.*, vol. 61, no. 12, pp. 2213–2216, 2017.
[61] N. Levin et al., "Remote sensing of night lights: A review and an outlook for the future," *Remote Sens. Environ.*, vol. 237, 2020, Art. no. 111443.
[62] L. Meng et al., "Artificial light at night: An underappreciated effect on phenology of deciduous woody plants," *PNAS Nexus*, vol. 1, no. 2, 2022, Art. no. pgac046.
[63] H. Du, M. Wang, Y. Liu, M. Guo, C. Peng, and P. Li, "Responses of autumn vegetation phenology to climate change and urbanization at northern middle and high latitudes," *Int. J. Appl. Earth Observ. Geoinf.*, vol. 115, 2022, Art. no. 103086.
[64] W. Jia, S. Zhao, X. Zhang, S. Liu, G. M. Henebry, and L. Liu, "Urbanization imprint on land surface phenology: The urban-rural gradient analysis for Chinese cities," *Glob. Change Biol.*, vol. 27, no. 12, pp. 2895–2904, 2021.
[65] S. Jochner, T. H. Sparks, J. Laube, and A. Menzel, "Can we detect a nonlinear response to temperature in European plant phenology?," *Int. J. Biometeorol.*, vol. 60, no. 10, pp. 1551–1561, 2016.
[66] H. Liu et al., "Nonlinear relationship of vegetation greening with nature and human factors and its forecast—A case study of Southwest China," *Ecol. Indicators*, vol. 111, 2020, Art. no. 106009.
[67] C. Santos, M. Salmerón, and Larry C. Purcell, "Soybean phenology prediction tool for the US midsouth," *Agricultural Environ. Lett.*, vol. 4, no. 1, 2019, Art. no. 190036.
[68] C. Xia, X. Gang, H. Xiaofei, and L. Danqi, "Influences of seasonal soil moisture and temperature on vegetation phenology in the Qilian mountains," *Remote Sens.*, vol. 14, no. 15, 2022, Art. no. 3645.

Jiahui Yao received the B.S. degree in remote sensing science and technology in 2021 from the School of Remote Sensing and Geomatics Engineering, Nanjing University of Information Science and Technology, Nanjing, China, where she is currently working toward the master's degree in resources and environment with the School of Remote Sensing and Geomatics Engineering.

Her research interests include vegetation phenological changes under climate change and urbanization.

Haiyong Ding received the bachelor's degree in mathematics education from Qufu Normal University, Jining, China, in 1998, the master's degree in operations research and control theory from the Shandong University of Science and Technology, Shandong, China, in 2004, and the Ph.D. degree in cartography and geographic information engineering from the China University of Mining and Technology, Jiangsu, China, in 2008.

He is currently a Professor with the School of Remote Sensing and Geomatics Engineering, Nanjing University of Information Science and Technology, Nanjing, China. His research interests include land use and land cover change, change detection, urban heat island, and land surface temperature.